J Neurophysiol 98: 744–756, 2007.
First published June 20, 2007; doi:10.1152/jn.01356.2006.

Temporal and Frequency Characteristics of Cartwheel Cells in the Dorsal Cochlear Nucleus of the Awake Mouse

Christine V. Portfors[1] and Patrick D. Roberts[2]

[1]*School of Biological Sciences, Washington State University, Vancouver, Washington; and* [2]*Neurological Sciences Institute, Oregon Health and Science University, Beaverton, Oregon*

Submitted 23 December 2006; accepted in final form 16 June 2007

Portfors CV, Roberts PD. Temporal and frequency characteristics of cartwheel cells in the dorsal cochlear nucleus of the awake mouse. *J Neurophysiol* 98: 744–756, 2007. First published June 20, 2007; doi:10.1152/jn.01356.2006. The dorsal cochlear nucleus (DCN) is an initial site of central auditory processing and also the first site of multisensory convergence in the auditory pathway. The auditory nerve imparts a tonotopic frequency organization on the responses of principal cells in the DCN. Cartwheel cells modify the responses of principal cells, but they do not receive direct auditory nerve input. This study shows that cartwheel cells respond well to tonal stimuli in the awake mouse and they have a well-defined characteristic frequency that corresponds to the tonotopic organization of the DCN. The auditory responses of cartwheel cells exhibit complex spectro-temporal responses to tones, with excitation and inhibition modulating the firing patterns in both frequency and time after onset of the stimulus. Temporal responses to best-frequency tones are highly variable between cartwheel cells, but a simple model is used to unify this variability as differences in the timing of synaptic currents. Cartwheel cell responses to two-tone stimuli show that interactions from different frequencies affect the output of cartwheel cells. The results suggest that at this primary auditory structure, processing of sound at one frequency can be modified by sounds of different frequency. These complex frequency and temporal interactions in cartwheel cells suggest that these neurons play an active role in basic sound processing.

INTRODUCTION

Many animals live in complex sensory environments and need to extract biologically relevant stimuli from a noisy background. For animals that utilize acoustic signals, detecting novel, important sounds from predictable background noise is an important task for survival. Separating important stimuli from background sounds early in the ascending auditory system would enhance efficiency of behavioral responses. The cochlear nucleus is the first site of auditory processing in the central auditory system and is a likely candidate for extraction of important sounds. In particular, the dorsal cochlear nucleus (DCN), as a cerebellum-like structure, may function as a novelty filter (Oertel and Young 2004). In DCN, the output neurons, fusiform and giant cells, receive input from auditory nerve afferents and parallel fibers. Parallel fibers originate in the granule cell domain and synapse onto fusiform, giant, and cartwheel cells in the superficial layer of DCN. The parallel fibers likely convey information from a wide range of auditory and nonauditory sources because the granule cell domain receives input from the auditory cortex (Weedman and Ryugo 1996), the inferior colliculus (Caicedo and Herbert 1993; Schofield and Cant 1999), the dorsal column nuclei (Li and Mizuno 1997), the pontine nuclei (Ohlrogge et al. 2001), and the trigeminal nucleus (Haenggeli et al. 2005; Li and Mizuno 1997; Zhou and Shore 2004). Thus the DCN is the first site of multimodal convergence in the auditory system and may play a significant role in auditory processing of complex sounds.

Cartwheel cells are interneurons whose cell bodies reside in the molecular layer of DCN (Berrebi and Mugnaini 1991). They do not receive primary afferents, but are excited by parallel fibers. Through the parallel fibers, cartwheel cells receive multisensory input, including auditory input from the auditory cortex (Weedman and Ryugo 1996), inferior colliculus (Caicedo and Herbert 1993; Schofield and Cant 1999), and possibly type II auditory nerve fibers (Brown et al. 1988) and VCN (Golding et al. 1995). Cartwheel cells project glycinergic input onto other cartwheel cells and onto fusiform cells (Golding and Oertel 1997). They may therefore act as a multimodal regulator of the DCN output, but their specific function in auditory processing is still unclear.

Cartwheel cells are easily distinguishable in vivo (Caspary et al. 2006; Davis and Voigt 1997; Davis and Young 1997; Parham and Kim 1995; Parham et al. 2000) and in vitro (Manis et al. 1994; Zhang and Oertel 1993a) by their complex-spiking patterns. Cartwheel cells have two types of spikes—simple spikes and complex spikes—whereas all other cell types in DCN exhibit simple-spiking patterns. The two spike types, and their inhibitory action on fusiform cells, qualify cartwheel cells as Purkinje-like cells in the DCN. Thus a better understanding of the function of cartwheel cells may reveal functional roles of similar cells in other cerebellum-like structures and in the cerebellum itself.

In addition, analogies with other cerebellum-like structures will suggest functional hypotheses to test in the DCN. For example, the initial stage of electrosensory processing in mormyrid electric fish (Bell et al. 1997) is a cerebellum-like structure that appears to be an adaptive filter to reduce the fish's sensitivity to expected somatosensory stimuli (Bell 1981). The analogous function for DCN would be to suppress predictable auditory signals and emphasize novel sounds.

However, because cartwheel cells in the DCN do not receive direct auditory nerve input and previous in vivo experiments have suggested that cartwheel cells are weakly driven or inhibited by tonal and broadband noise stimuli and often do not

Address for reprint requests and other correspondence: C. V. Portfors, School of Biological Sciences, Washington State University, Vancouver, WA 98686 (E-mail: portfors@vancouver.wsu.edu).

The costs of publication of this article were defrayed in part by the payment of page charges. The article must therefore be hereby marked "*advertisement*" in accordance with 18 U.S.C. Section 1734 solely to indicate this fact.

have well-defined characteristic frequencies (Davis and Young 1997; Parham and Kim 1995; Parham et al. 2000), it has been difficult to link the function of the DCN to a general auditory processor in analogy to the electrosensory system. Here we present evidence that the cartwheel cells in the awake mouse respond well to tones, have clear frequency tuning, and have a tonotopic organization similar to the somatotopic organization of the early electrosensory system. This new finding strengthens the analogy between the two systems and allows us to make further predictions about how cartwheel cells may adaptively control the output of the DCN.

In addition, because the evoked responses of the cartwheel cells in awake mouse were somewhat complex, we developed a quantitative model to predict the timing of complex and simple spikes. The model revealed that the membrane properties of cartwheel cells could explain the pattern of spikes that we observed in the awake mouse. The model also predicted the timing of parallel fiber activity that carries auditory information. Because of the known adaptive properties of neurons in this cerebellum-like structure and their similarity to neurons in the electrosensory system, we suggest that the DCN provides an adaptive filtering of pure auditory stimuli for modulation of predictable temporal patterns in the auditory environment.

METHODS

Electrophysiology methods

We recorded responses of cartwheel cells in the DCN of CBA/CaJ mice to pure tone stimuli.

SURGICAL PROCEDURES. To enable recordings from single units in the awake mouse, we attached a metal pin onto the skull and bolted this pin to a custom-made stereotaxic apparatus during recordings. The pin was attached 1 or 2 days before electrophysiological recordings. To attach the headpin, the animal was anesthetized with isoflurane inhalation and placed in a rodent stereotaxic frame with a mouse adaptor. Ear bars were used to hold the head firmly during surgery. Care was taken to prevent damage to the tympanic membrane. To expose the skull, a midline incision was made in the scalp and the skin reflected laterally. The pin was cemented onto the skull using ultraviolet-cured dental cement. A tungsten ground electrode was cemented into the right cerebral cortex. Using stereotaxic coordinates from the mouse brain atlas (Paxinos and Franklin 2001), a craniotomy was made with a scalpel over the cerebellum to access the DCN. The location of the craniotomy was between 5.6 and 6.3 mm caudal to the bregma line and between 2.0 and 2.6 mm from the midline. This location allowed a straight dorsal-to-ventral approach to the DCN. The superficial layer of DCN was encountered at a depth of approximately 2.8 mm from the dorsal surface of the brain. A local anesthetic (lidocaine) and a topical antibiotic (Neosporin) were applied to the wound after the surgery and the animal was returned to its home cage for at least 1 day before electrophysiological recordings.

ACOUSTIC STIMULATION. Pure-tone stimuli were synthesized using custom-written C++ computer algorithms. Sound stimuli were output through a high-speed, 16-bit D/A converter (Microstar Labs; 400,000 samples/s), fed to a programmable attenuator (Tucker Davis Technologies PA5), a power amplifier (Parasound), and to a leaf tweeter speaker located 10 cm away from the mouse. The acoustic properties of the system were regularly tested using a 1/4-in. calibrated microphone (Brüel & Kjær, model 4135) placed in the position normally occupied by the animal's ear. There was a smooth, gradual decrease in sound pressure from 6 to 60 kHz of about 2.7 dB per 10 kHz. Distortion components were buried in the noise floor, $\geq$50 dB below the signal level, as measured by custom-designed software performing a fast Fourier transform of the digitized microphone signal.

EXTRACELLULAR RECORDING PROCEDURE. During extracellular recordings, the awake animal was restrained in a piece of foam molded to its body, and its head was maintained in a uniform position by attaching the pin on the mouse's head to a bar on a custom-designed stereotaxic apparatus. The animal was lightly sedated with acepromazine to put it into the stereotaxic apparatus. Animals that struggled during the experiments were removed for the day and returned to their home cages. The stereotaxic apparatus was placed on an air table in a single-walled sound-attenuating chamber that was covered with acoustic foam. If recording sessions continued for >4–5 h, the mouse was returned to its cage for a 1-h break halfway through the session. During the recording session, the experimenter offered the mouse water from a dropper after each electrode penetration, which was typically 1–2 h. Experiments lasted between 1 and 3 days. Petroleum jelly was used to protect the exposed brain between recording sessions.

To obtain well-isolated single-unit responses, we used micropipettes filled with 1 M NaCl (resistances of 20–30 MΩ). Electrodes were advanced by a hydraulic micropositioner (David Kopf Instruments) located outside the acoustic chamber. Extracellular action potentials were amplified (Dagan), filtered (band-pass, 500–6,000 Hz; Krohn-Hite), and sent through a spike enhancer (FHC) before being digitized (Microstar Laboratories, 10,000 samples/s). Individual neural waveforms were displayed and archived using custom-written C++ software. The software displayed raster plots, poststimulus time histograms (PSTHs), and statistics on-line. Spike discrimination, spike enhancement, and time-window analysis parameters could be altered off-line to analyze stored raw waveforms. Raster and PSTH data as well as latencies were output in ASCII format for further data analysis using custom routines written for Matlab (The MathWorks, Natick, MA) and IGORPro (WaveMetrics, Lake Oswego, OR) software.

Broadband noise (BBN, 10–100 kHz, 100 ms in duration) was used as a search stimulus. Once a single unit was isolated, we used single-tone burst stimuli to quantitatively examine excitatory frequency response areas throughout most of the mouse's audible range. Characteristic frequency (CF) and minimal threshold (MT) were determined audiovisually and confirmed with quantitative frequency tuning tests. The CF was defined as the frequency at which a unit fired evoked spikes to $\geq$50% of the stimulus presentations at threshold, and threshold was defined as the minimum intensity required to evoke a response to 50% of the stimuli at the CF. Frequency response maps were generated by presenting tones (100-ms duration, 1-ms rise/fall time, 3/s, 300-ms recording window) across the majority of the mouse hearing range (6–60 kHz in 2-kHz steps) in 10- to 20-dB intensity steps from 10 dB above threshold to about 80 dB SPL. Each frequency–intensity pair was presented 20–25 times. We presented tones in linear steps so that all frequencies across the animals' hearing range had equal resolution.

Rate/level functions were obtained for CF tones and BBN. Twenty-five repetitions of the CF tone were first collected in 10-dB intensity steps starting at threshold. Then responses to a 100-ms BBN stimulus (1-ms rise/fall, 3/s, 300-ms recording window) were collected at the same intensity levels as used in the tone test.

Twenty-five repetitions of no stimulus were used to calculate spontaneous rate. In neurons with high spontaneous rates, inhibitory areas were obtained from the single-tone tests. In neurons with no or low spontaneous activity, inhibitory areas were characterized from a two-tone test. In this test, a CF tone was presented at 10–20 dB above threshold to generate a consistent excitatory response while a second tone with simultaneous onset that varied in frequency and intensity was presented. Frequencies that suppressed the CF excitatory response constituted the inhibitory response area of that neuron.

To obtain temporal discharge patterns and median first-spike latencies, 200 repetitions of a CF tone at 30 dB above threshold were presented and PSTHs constructed.

Data were analyzed only from single units judged to be cartwheel cells based on previously published criteria (Caspary et al. 2006; Davis and Voigt 1997; Ding et al. 1999; Parham and Kim 1995; Parham et al. 2000). To be included in the analysis, each single unit had to have the following features: *1*) complex spikes; *2*) superficial recording site in the DCN (compared with units displaying characteristics of fusiform cells); *3*) bimodal temporal firing pattern to CF in which complex spikes were followed by simple spikes; and *4*) long and variable first-spike latencies (compared with first-spike latencies of units displaying characteristics of fusiform cells). Data were analyzed using custom routines written in IGORPro (WaveMetrics). To compare temporal firing patterns of complex spikes and simple spikes obtained from empirical experiments with those obtained from our mathematical model, PSTHs and rasters were run through a custom-written program to color-code complex and simple spikes; complex spikes were reduced to a single spike and colored red and simple spikes were colored black. For analyses of frequency tuning, complex spikes were not reduced to one spike in PSTHs.

All electrophysiological procedures were in strict accordance with the National Institutes of Health Guide for the Care and Use of Animals and were approved by the Washington State University Institutional Animal Care and Use Committee.

Mathematical methods

We combined our electrophysiological methods with mathematical modeling to unify the physiological responses of cartwheel cells, and to predict the synaptic currents that explain the temporal patterns of complex and simple spikes in response to auditory stimuli.

QUANTITATIVE CARTWHEEL CELL MODEL. Our aim was to construct a cartwheel cell model that would be complex enough to represent both simple and complex spikes, but not too complex to hide the mechanisms of spike generation. Nonlinearities of voltage-dependent membrane currents in cartwheel cells, and their morphology, may affect the resulting spatiotemporal spike patterns that result from synaptic inputs and dendritic filtering. However, a simple model with dynamics that can be easily analyzed will help to tease apart the effects arising from intrinsic properties of cartwheel cells from the effects arising from synaptic input patterns. Therefore we applied a dynamical systems approach and constructed a single-compartment, two-dimensional integrate-and-fire (2D-IF) model (Izhikevich 2003, 2006) that was based on the dynamics of the membrane currents. The two variables of the model cartwheel cell were the membrane potential v and a slow "recovery" variable u. In this type of model, a fast spike is terminated when the v-variable crosses a preset threshold and the two variables are reset.

Complex spikes in cartwheel cells are driven by a slow, Ca^{2+}-based plateau (Manis et al. 1994; Zhang and Oertel 1993a). Fast, sodium-dependent spikes ride on top of the plateau potential (Golding and Oertel 1997), and the complex-spike burst is presumably terminated by the activation of a calcium-dependent potassium current. In the topological classification of Izhikevich (2006), a complex-spike burst mechanism leads to a fold/homoclinic bifurcation. A fold bifurcation pushes the trajectory into a cycle around an unstable focus. Each cycle around the unstable focus (each spike) increments a slow, recovery variable that eventually repolarizes the cell and terminates the burst.

We represented the bursting dynamics with a two-state, resetting (integrate-and-fire) model

$$C_m\dot{v} = k(v_r - v)(v_t - v) - u + I \quad (1)$$

$$\dot{u} = a[b(v - v_r) - u] \quad (2)$$

If $v \geq v_{peak}$, then $v \rightarrow c$ and $u \rightarrow u + d$.

The parameters were set to the following values: $C_m = 50$ pF, $v_r = -65$ mV, $v_t = -35$ mV, $k = 1$, $v_{peak} = 0$ mV, $a = 0.03$, $b = 10$, $c = -40$, and $d = 100$. These parameters were arrived at by starting from a bursting cell model from Izhikevich (2006), and then adjusting the parameters until obtaining both simple spikes and bursts with only two to three spikes that would represent complex spikes. In addition, the equilibrium potential v_r was chosen to be close to actual cartwheel cells (Golding and Oertel 1997).

Synaptic inputs to the 2D-IF models were represented as a sum of N postsynaptic currents, $I(t) = \sum_{i=1}^{N} I_i(t)$, where $I_i(t) = g_i(t)[V(t) - E_r]$ and E_r is the reversal potential. The synaptic conductance $g_i(t)$ was calculated by $g_i(t) = g^i_{max} r_i(t)$, which describes the kinetics of the synaptic currents. We used a linear Markov model to calculate the conductance, where $r_i(t)$ represents the open probability of the synaptic channels. In our model, $r_i(t)$ was a single variable (two states: open and closed) to represent currents from α-amino-3-hydroxy-5-methyl-4-isoxazolepropionic acid receptors (Destexhe et al. 1994) and $r_i(t)$ was described by the equation, $\dot{r}_i = \alpha T(1 - r_i) - \beta r_i$. The transmitter variable T was reset $T \rightarrow T_{max}$ only if there was a presynaptic spike; otherwise, $T = 0$. Each model synapse had $T_{max} = 0.1$ and $E_r = 0$ mV. A series of synaptic inputs were used in simulations to estimate the parallel fiber inputs to cartwheel cells in vivo (see RESULTS).

The differential equations of the model were integrated numerically to simulate the response of cartwheel cells to current injections. The response to a current step is shown in Fig. 1*A*, where $I(t) = 1$ nA for 20 ms $\leq t \leq$ 170 ms, and $I(t) = 0$ otherwise. The variables are initiated at equilibrium ($v = -65$ mV and $u = 0$ nA). A current step at $t = 20$ ms generates a complex spike yielding two fast spikes, and then the plateau is terminated to be followed by a simple spike at 100 ms. The step current is large enough to generate a series of simple spikes, but in this example we terminate the current at $t = 170$ ms and the variables return to equilibrium.

The reason for the initial complex spike followed by simple spikes is evident in the trajectory in the u–v plane (Fig. 1*A*, *bottom*). Initially, the variables are stationary at their equilibrium (Fig. 1*A*, *bottom*, eq), which is a stable fixed point at the intersection of the v-nullcline

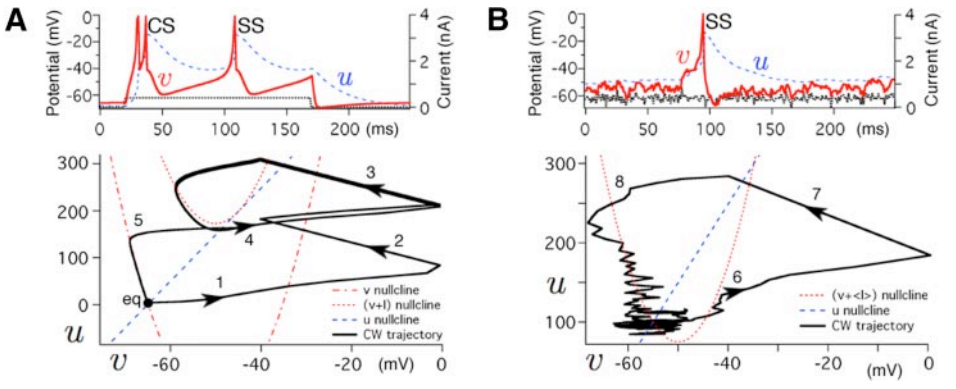

FIG. 1. Simulation of a one-compartment, 2-dimensional, integrate-and-fire cartwheel cell. *A*: model variables, v (solid red) and u (dashed blue; u is scaled by a factor of 10) in response to a current step (dotted black) lasting 150 ms. Two types of spikes are present: the initial complex spike (CS) and a late simple spike (SS). *Bottom*: trajectory (solid black) of the *top trace* in the u–v plane. *B*: model responds with a simple spike to a noisy current injection. *Bottom trace*: trajectory in the u–v plane (see text for details).

(dot-dashed parabola) with *u*-nullcline (dashed line). The current step shifts the *v*-nullcline to a new position (dotted parabola) where the intersection of nullclines is no longer a stable fixed point. The trajectory then increases *v* (Fig. 1*A*, *bottom*, 1) until $v = 0$, where *v* is reset to −40 mV and *u* is incremented by 100 pA (Fig. 1*A*, *bottom*, 2). However, this reset has not pushed the trajectory into a region of the *u*–*v* plane where the dynamics would drive the variables toward lower values (left of the *u*-nullcline and above the *v*-nullcline). Thus a second fast spike is initiated to be reset (Fig. 1*A*, *bottom*, 3) into a region that terminates the complex spike. The position of the *v*-nullcline does not yet support a stable fixed point and a new spike is initiated (Fig. 1*A*, *bottom*, 4), but now the *u*-variable is sufficiently large that the reset shifts the trajectory into a region that reduces both variables, resulting in a simple spike. Before a second simple spike is initiated, the current step ceases, the *v*-nullcline shifts back to the lower position (dot-dashed parabola), and the trajectory (Fig. 1*A*, *bottom*, 5) falls into the attractor basin of the stable fixed point (Fig. 1*A*, *bottom*, eq).

If the injected current increased slowly, instead of a step-current injection, the *u*-variable would have time to adjust and only simple spikes would result because the equilibrium of the system would shift as the *v*-nullcline was elevated until the fixed point became unstable. Then the system would be in the position (Fig. 1*A*, *bottom*, 4) so that the reset of *v*, and increment of *u*, would push the variables above the *v*-nullcline to repolarize the cartwheel cell, terminating the "burst" after one simple spike.

Another example is shown in Fig. 1*B*, but in this case simple spikes dominate the depolarizations. Current is injected with zero mean and a variance of 120 pA. The noisy current results in a jittering of the variables near their mean equilibrium value. Occasionally, the variables cross the *v*-nullcline (Fig. 1*B*, *bottom*, 6) leading to a fast spike and resetting (Fig. 1*B*, *bottom*, 7) of *v*. However, in this case the reset pushes the variables into the attractor basin of the stable equilibrium (Fig. 1*B*, *bottom*, 8), and the membrane potential repolarizes after the reset, resulting in a simple spike.

RESULTS

We recorded auditory responses from 77 single units in the DCN. Twenty-one single units were classified as cartwheel cells based on the previously defined criteria. The remaining cells exhibited only simple spikes. The response characteristics of these units are not described herein, other than to use some of their response features as a comparison to the complex-spiking cartwheel cells. The complex-spiking patterns of cartwheel cells were easily distinguishable from simple-spiking cells. Figure 2 shows waveforms of two cartwheel cells recorded from the DCN of awake mouse. These cells are typical, rather than exceptional, examples of signal-to-noise levels in our single-unit recordings. The first spike in response to sound shows the characteristic bursting pattern of complex spikes (CS) recorded from cartwheel cells intracellularly in the DCN (Davis and Voigt 1997; Manis et al. 1994; Tzounopoulos et al. 2004; Zhang and Oertel 1993b).

Cartwheel cells were found in the superficial region of the DCN, corresponding to the location of cartwheel cell bodies in the molecular layer. The average recording depth (zero is at electrode insertion into cerebellum) of cartwheel cells in our sample was 3,025 μm, compared with 3,369 μm for simple-spiking neurons. Because the start of the DCN was located 2,800 μm from the surface of the brain, the depth of the cartwheel cell recordings were all within the superficial 580 μm of the DCN.

Temporal firing patterns of cartwheel cells are bimodal

Along with complex-spiking patterns, cartwheel cells often had distinct temporal firing patterns. PSTHs in Fig. 3 show the temporal firing characteristics of four cartwheel cells. In these cells, complex spikes were differentiated from simple spikes based on interspike interval. The multiple spike times of the complex spikes were reduced to one spike time and plotted in red to easily distinguish the firing patterns of the different types of spikes. One feature that was common in the cartwheel cells firing pattern was that the initial complex spike (CS) was followed by a pause and then a simple spike (SS) (see waveforms in Fig. 2, PSTHs in Fig. 3). This temporal firing pattern shows up as a bimodal spike distribution. Simple-spiking neurons did not show this bimodal type of spike distribution.

A second characteristic temporal feature of cartwheel cells was their long and variable latency compared with that of simple-spiking neurons. Latency was measured as the median latency of the first spike in 25 presentations of the CF tone presented at 30 dB above threshold. The mean (SD) latency of complex-spiking units was 30.8 ms (14.2 ms) compared with values between 8.3 ms (3.5 ms) and 11.5 ms (5.6 ms) for the other unit types in our sample. This longer latency of cartwheel cells corresponds well with cartwheel cells not receiving direct, afferent input from the auditory nerve. In addition, cartwheel cells tended to have low rates of spontaneous activity (mean 7.8, SD 5.8 spikes/s).

Unimodel synaptic inputs are sufficient to explain bimodal firing patterns

To explain the bimodal firing patterns in cartwheel cells, we constructed a 2D-IF model (*Eqs. 1* and *2*) that would simulate both simple spikes and spike bursts indicative of complex spikes. The interpretation of these spiking dynamics in terms of ion currents in cartwheel cells (Kim and Trussell 2007) is that the *u*-variable is related to a slow, hyperpolarizing current that is incremented by depolarizations, and decays on a slower timescale than the fast currents. Fast sodium spikes are represented by the increasing of *v* due to the quadratic force on the right-hand side of *Eq. 1*, and the subsequent resetting of *v* that represents a delayed rectifier potassium current. By incrementing *u*, we represent the influx of calcium ions, by high-threshold calcium channels, that lead to the activation of a slow, calcium-activated potassium current. When the cartwheel cell is at rest with no current injection, the levels of calcium have been low and the slow potassium current is inactive ($u =$

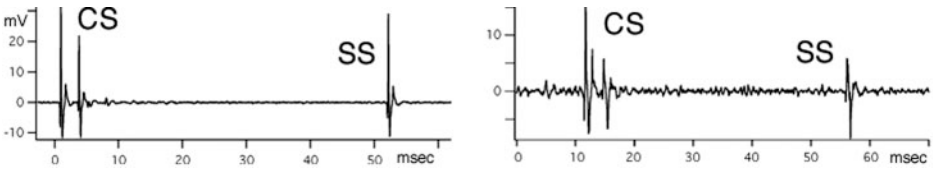

FIG. 2. Cartwheel cells respond well to sound in our awake mouse preparation. Waveforms recorded and stored off-line of 2 cartwheel cells show complex spikes (CS) and simple spikes (SS) to sound stimulation. Note the time delay between the CS and SS in both units.

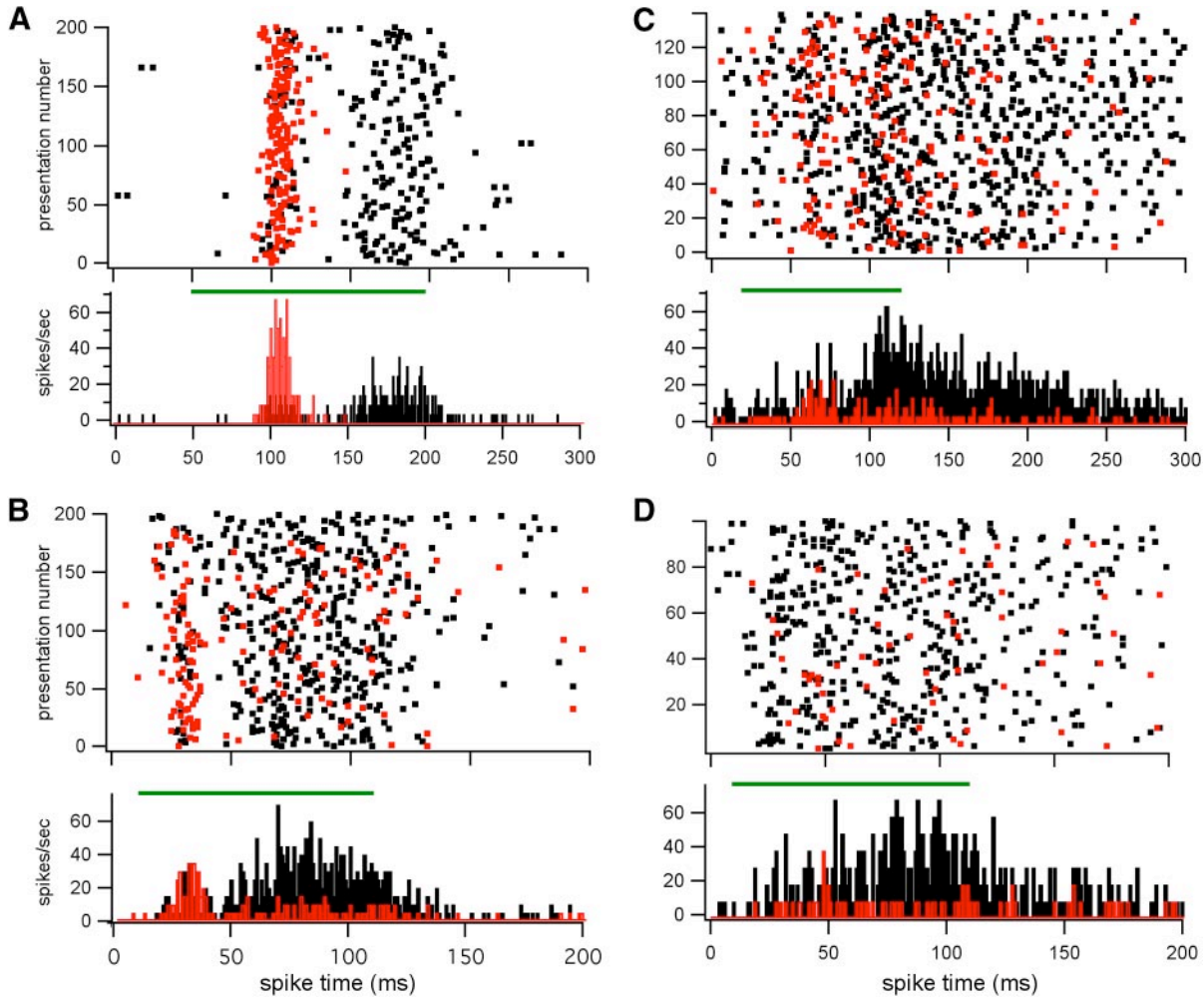

FIG. 3. Temporal firing patterns of cartwheel cells show bimodal distribution of complex and simple spikes. *A–D*: spike patterns of complex spikes (red) and simple spikes (black) of 4 cartwheel cells. All spikes in the complex spike are reduced to one spike and colored red. Spike rasters and their corresponding poststimulus time histograms (PSTHs) were obtained to characteristic frequency (CF) tone at 30 dB above threshold. Horizontal bar at *top* of PSTH denotes stimulus onset and duration. *A*: this unit had a CF of 15 kHz and a threshold of 24 dB SPL. *B*: this unit had a CF of 32 kHz and a threshold of 25.5 dB SPL. *C*: this unit had a CF of 17 kHz and a threshold of 28 dB SPL. *D*: this unit had a CF of 19 kHz and a threshold of 31 dB SPL.

0). A current step initiates a complex spike because the system requires two sodium spikes to activate enough slow, calcium-activated potassium channels to repolarize the membrane potential. After the initial complex spike, there is enough residual calcium and slow calcium-activated potassium current to sufficiently repolarize the cell after a single sodium spike so that only simple spikes are generated.

We used the 2D-IF model cartwheel cell to predict auditory responses recorded in vivo by representing synaptic currents that could be distributed in time to simulate parallel fiber responses to an auditory stimulus. By varying the distribution of the spike timings and synaptic strengths in a population of parallel fiber inputs, we could replicate the complex- and simple-spike patterns observed during auditory stimuli. The results predict the parallel fiber spike pattern in DCN that results from auditory stimuli.

In our simulations, a series of N synaptic currents were injected into the model cartwheel cell to represent parallel fiber activity that results from auditory stimulation. The maximum synaptic current was graded throughout the stimulus cycle to represent the temporal pattern of synaptic currents. Thus when we matched the complex- and simple-spike patterns with a cartwheel cell recorded in vivo, we arrived at a prediction of the synaptic currents that generated the spike pattern.

Simulated cartwheel cell spike patterns are shown in Fig. 4. This example had a series $N = 150$ parallel fiber synapses beginning at 30 ms after the start of the stimulus cycle. The maximum synaptic current for each model synapse was $g^i_{max} = 0.6i/t_{peak}$ for $i \leq t_{peak}$, and $g^i_{max} = 0.6(N - i)/(N - t_{peak})$ for $i > t_{peak}$, where i denotes the synapse that fired at time i ms after the start of the stimulus cycle and t_{peak} denotes the peak synaptic current during the cycle. The synaptic currents of the model were adjusted for Fig. 4*A* to fit the data in Fig. 3*A*, and then only the value of t_{peak} was increased to yield the other patterns. The model cartwheel cell responded with long-latency complex spikes followed by simple spikes as was consistent with our recordings of cartwheel cells (Fig. 3) for different values of t_{peak}. These simulations demonstrate that a unimodel excitatory input pattern from parallel fibers, in combination with the complex-spike–bursting property of cartwheel cells, is sufficient to explain the bimodal spike patterns. In addition, different profiles of the synaptic current from parallel fibers were sufficient to explain all of the observed spike patterns from cartwheel cells.

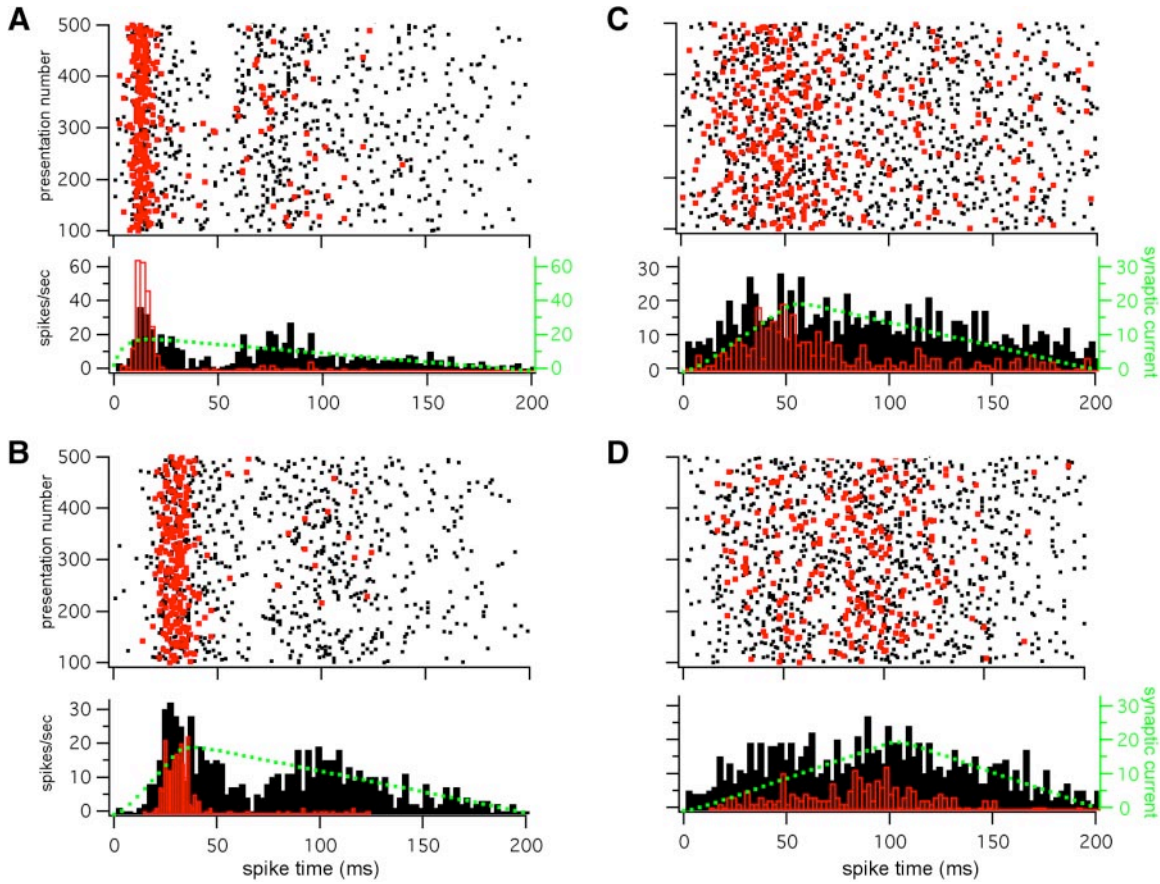

FIG. 4. Two-dimensional integrate-and-fire (2D-IF) cartwheel cell model with synaptic currents simulates in vivo responses to auditory stimuli. *A–D*: spike patterns (CS, red; SS, black) generated by excitatory postsynaptic currents (*dotted green trace* superimposed on PSTH) shown here in a "voltage-clamped" configuration. All of the spike patterns observed in vivo (see Fig. 3) can be explained by different timings of maximal postsynaptic currents. Bimodel patterns (*A* and *B*) are caused by an initial strong input, whereas the unimodel patterns (*C* and *D*) are generated by a more gradual increase of synaptic currents during the stimulus cycle.

Our model allows us to predict the synaptic current into cartwheel cells during auditory stimuli. The latencies of the first spikes in the response yield a prediction of the latencies of synaptic currents. The example in Fig. 3*A* suggests a synaptic current latency of about 50 ms. Figure 3, *B–D* suggests latencies of <50 ms. A significant delay between the beginning of the excitatory synaptic current and the first spike is inherent in the model dynamics because of the slow buildup of the membrane potential to initiate a spike. These modeling results suggest that the bimodal latency distribution of cartwheel cell spikes during auditory stimuli is due to unimodal synaptic inputs, and the observed temporal relationship between complex and simple spikes is due to membrane properties of cartwheel cells.

Frequency tuning of cartwheel cells is broad but consistent

Previous studies of cartwheel cells in vivo have suggested that many cartwheel cells respond weakly or are inhibited by tones and often a best frequency cannot be determined (Davis and Young 1997; Parham and Kim 1995; Parham et al. 2000). In contrast, we were able to determine a best frequency for all 21 complex-spiking units in this study. The range of characteristic frequencies was 11–33 kHz (Fig. 5), with most CFs between 16 and 20 kHz. The range of thresholds at CF was 15–56 dB SPL (Fig. 5*A*) with a mean (SD) of 33 (11) dB SPL. These thresholds were only slightly higher than thresholds of principal cells in the DCN recorded from the same mouse preparation [type II: 29 (12) dB SPL; type III: 25 (14) dB SPL; type I/III: 26 (19) dB SPL]. However, they are lower than thresholds cited for cartwheel cells in anesthetized mouse (range between 0 and 70 dB SPL) (Parham et al. 2000).

The characteristic frequency of the cartwheel cells was consistent with their location with respect to the tonotopy of the DCN. Thus there seems to be an organization of cartwheel cells based on their CF. In the DCN, high frequencies are represented dorsally and lower frequencies are represented more ventrally. In dorsoventral penetrations through the DCN, cartwheel cells were recorded dorsally, as was expected, because of their cell bodies being located in the molecular layer. However, we did not expect the CFs of the units to follow the tonotopy of the DCN because the parallel fibers traverse perpendicular to the isofrequency contours. Figure 5*C* illustrates the CF of each cartwheel cell plotted versus the CF of the closest unit in the same electrode penetration (i.e., the "nearest neighbor"). Although the nearest neighbor may have been ≤200 microns away from the cartwheel cell, the CFs of the neurons are very similar, suggesting that there is an organization of the cartwheel cells based on frequency.

Frequency tuning tended to be broad in cartwheel cells. Figure 5*B* shows sharpness of frequency tuning quantified by

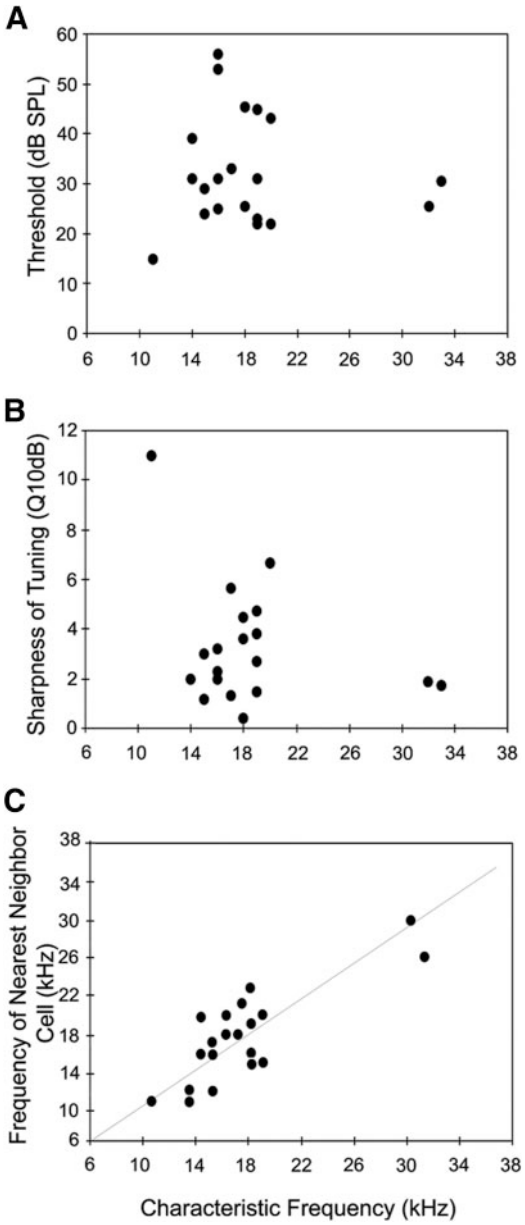

FIG. 5. Cartwheel cells in awake mouse dorsal cochlear nucleus (DCN) respond well to sound and show tuning to frequency. *A*: CF vs. threshold of cartwheel cells. CFs ranged between 11 and 32 kHz with thresholds between 15 and 56 dB SPL. *B*: sharpness of tuning was quantified by the Q10dB value and plotted vs. CF. *C*: cartwheel cells were organized in frequency in a similar manner to the tonotopic organization of the DCN. CF of each neuron plotted vs. the CF of the next nearest neighbor in the same electrode penetration. CFs of the cartwheel cell and the next neuron were very similar, suggesting an organization to the frequency tuning characteristics of the cartwheel cells. Diagonal line represents where data points would fall if CFs of cartwheel cells and their nearest neighbor cell were identical.

Q10dB values plotted versus CF. Q10dB was determined by dividing the characteristic frequency of the unit by the bandwidth of the frequencies that elicited a response rate that was 20% above the spontaneous rate at 10 dB above the unit's threshold. The mean (SD) Q10dB value for the cartwheel cells was 3.3 (2.4).

Evoked responses of cartwheel cells were often complex such that standard frequency response maps did not clearly illustrate frequency tuning characteristics (Fig. 6). To examine frequency tuning of cartwheel cells in more detail, we plotted frequency response areas as spectrotemporal histograms. In this type of plot, frequency and temporal information is retained with time on the *x*-axis and frequency of sound stimulation on the *y*-axis. The grayscale of each row represents the PSTH for the corresponding frequency. Spectrotemporal histograms are displayed for eight cartwheel cells in Figs. 7–10. These examples were chosen to show the variety of cartwheel cell responses and to identify the types of responses observed in our sample.

The units in Fig. 7 had sharp frequency tuning. The CFs and thresholds were 18 kHz, 45 dB SPL; 17 kHz, 28 dB SPL; and 20 kHz, 43 dB SPL and the Q10dB values were 3.6, 5.6, and 6.6, respectively. The broadness of the frequency response did not increase much as the intensity was increased and the latencies of the excitation phase of the response were rather consistent in each of these examples. However, other temporal aspects of the response patterns were noticeably altered. The unit in Fig. 7*A* developed a strong, late inhibition of the spontaneous activity at higher intensities. The inhibition outlasted the repetition rate of the stimulus presentation (three repetitions/s) at the highest intensity. The unit in Fig. 7*B* lengthened the duration of excitation and developed sideband inhibition at higher intensities, whereas the unit in Fig. 7*C* shortened the duration of excitation and developed a late inhibition.

The units in Fig. 8 had broader, V-shaped tuning. As intensity was increased, the frequency response areas expanded both above and below the CF. The CFs and thresholds of the units in Fig. 8 were 19 kHz, 31 dB SPL and 15 kHz, 24 dB SPL. Their frequency tuning was broad with

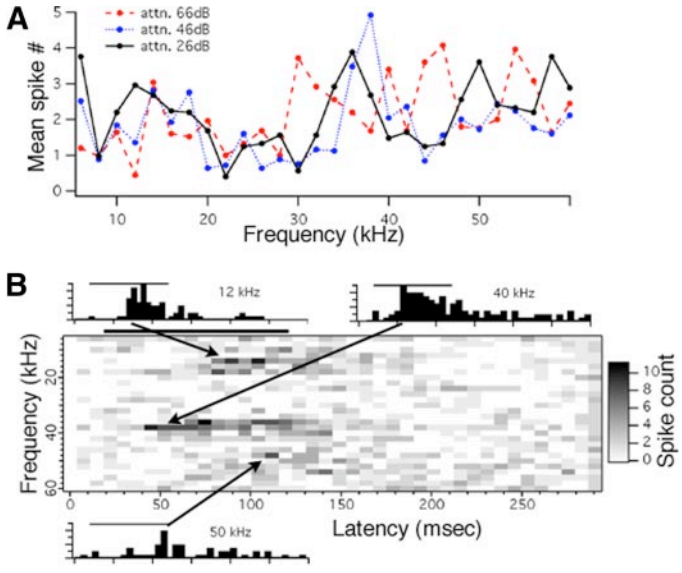

FIG. 6. Cartwheel cells in awake mouse DCN have complex frequency tuning that often is not well illustrated in standard frequency response maps. *A*: frequency response maps at 3 levels of intensity. Frequency response of the unit is not easily distinguishable from the response map. *B*: spectrotemporal histograms with select PSTHs shown in detail (bin width = 7 ms). In this type of plot, frequency and temporal information is retained with time on the *x*-axis and frequency of sound stimulation on the *y*-axis. Each row represents the PSTH for the corresponding frequency. Clear excitatory responses at 12 and 40 kHz with inhibition in between can be seen in the spectrotemporal histogram. This frequency tuning is apparent only in our spectrotemporal plot and not in commonly used response maps. Spectrotemporal histogram is at the middle attenuation value from *A*.

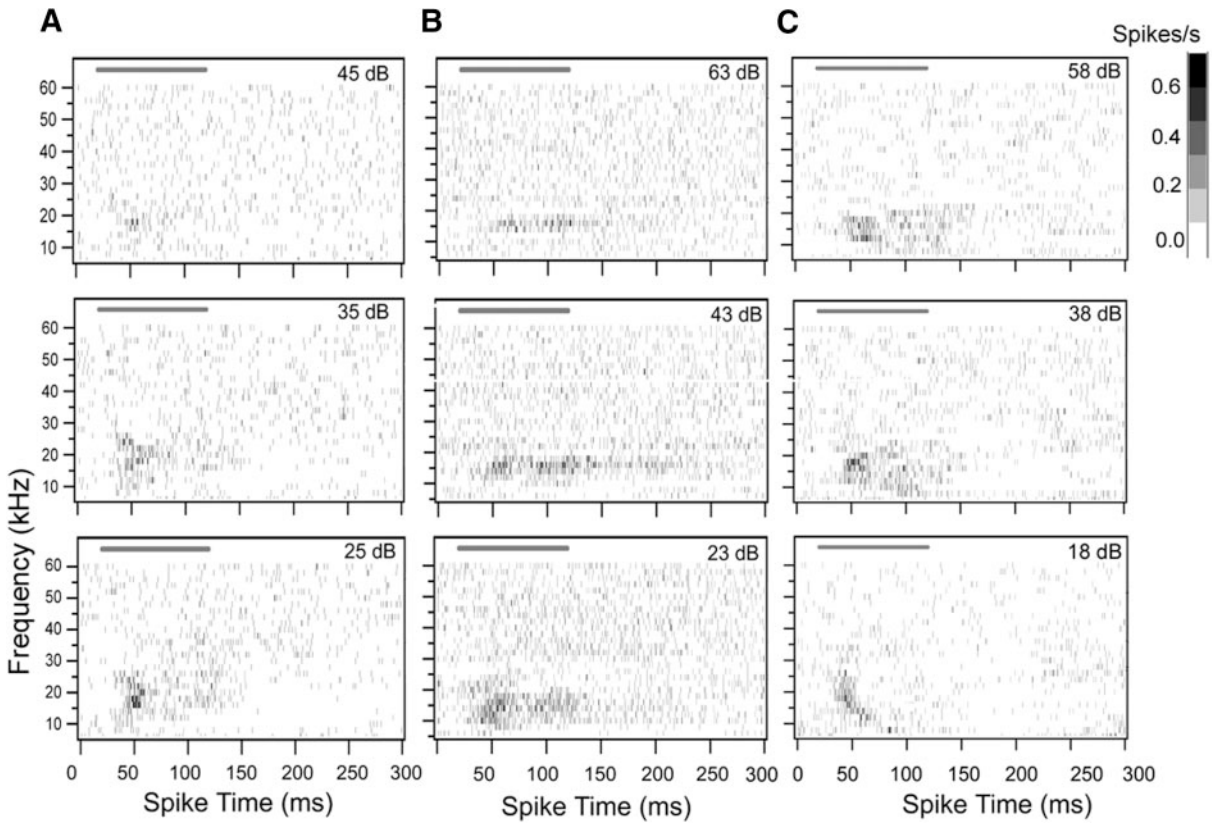

FIG. 7. Some cartwheel cells were sharply tuned in frequency. *A–C*: spectrotemporal histograms of 3 cartwheel cells at varying intensities. Intensity is shown as dB attenuation due to the speaker output not being flat across all frequencies tested. In these plots, the grayscale of each row represents the PSTH for the corresponding frequency. Darker gray denotes greater spike rate as indicated by the scale bar in the right-hand side of the figure. *A*: CF of this cell was 18 kHz, the threshold was 45 dB SPL, and the Q10dB was 3.6. *B*: CF of this unit was 17 kHz, the threshold was 28 dB SPL, and the Q10dB was 6.6. *C*: CF of this unit was 20 kHz, the threshold was 43 dB SPL, and the Q10dB was 6.6.

Q10dB values of 1.5 and 3.0, respectively. The two units in Fig. 8 also differed in that the unit of *B* developed a late inhibition at higher intensities that outlasted the repetition rate (two repetitions/s). The unit also showed a sharpening of the early spikes of the excitatory phase, but our model supports the possibility that the sharpness would be magnified by the inhibition and, consequently, this effect may disappear as slower repetition rates.

Auditory responses exhibit complex patterns of excitation and inhibition

The unit in Fig. 9 had two frequency response areas. One excitatory region was centered at 16 kHz and the second at 38 kHz. The suppression of spontaneous activity between the two excitatory response areas indicates that inhibition separated the two response areas. This was the only example of multiple tuning in our sample of cartwheel cells.

Inhibitory frequency response areas were determined from two-tone tests or by suppression of spontaneous activity. Two cells with inhibitory response areas are displayed in Fig. 10. The cell in Fig. 10*A* had a CF of 19 kHz and a threshold of 23 dB SPL. It had long-lasting inhibition after the excitatory response that wrapped around the recording duration to inhibit spontaneous activity before the stimulus onset. In addition, there was an inhibitory region above CF at high intensities. The unit in Fig. 10*B* had a CF of 32 kHz and a threshold of 25 dB SPL. It had inhibitory sidebands on both the high- and low-frequency sides of CF as well as inhibition following the excitatory response. In our sample of 21 cartwheel cells, eight had inhibitory frequency response regions.

Besides low thresholds and clear frequency tuning, another indication that the cartwheel cells in our awake mouse preparation had excitatory and inhibitory frequency interactions was their better responses to CF tones compared with broadband noise. Figure 11 shows a PSTH generated from responses to CF tones and BBN at the same intensity levels for a cartwheel cell. Threshold to the CF tone was 35 dB lower than threshold to BBN in this example. Mean (SD) threshold for CF tones was 33 (11) dB SPL and 61 (13) for BBN. These data indicate the complex interactions between excitatory and inhibitory inputs in cartwheel cells.

DISCUSSION

A major finding of this study is that cartwheel cells in the DCN of the awake mouse respond well to auditory stimuli and have a clear, and sometimes complex, frequency tuning. These findings are in contrast to previous studies of DCN that suggest cartwheel cells respond weakly or are inhibited to tones and often do not show clear frequency tuning (Davis and Voigt 1997; Parham and Kim 1995; Parham et al. 2000; Young and Davis 2002). The responsiveness of cartwheel cells to auditory stimuli may be underestimated in previous studies because many recordings have been in decerebrate animals (Davis and Voigt 1997; Davis and Young 1997; Parham and Kim 1995;

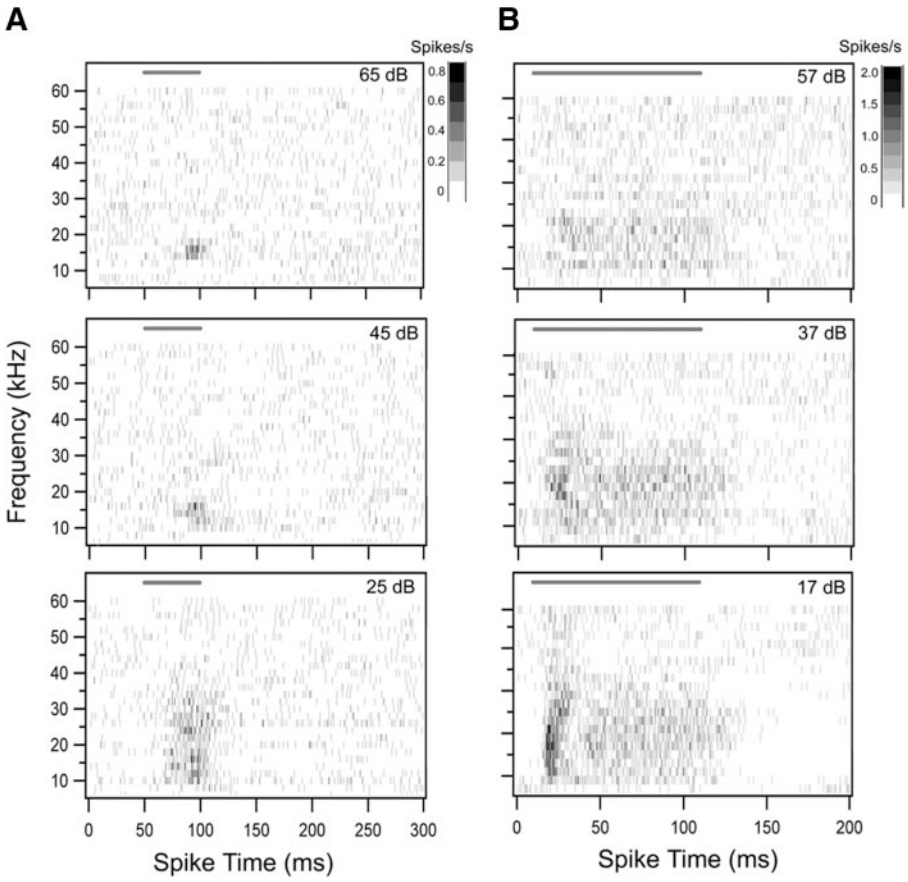

FIG. 8. Some cartwheel cells had broad, V-shaped tuning curves. *A* and *B*: spectrotemporal histograms of 2 cartwheel cells. Details of plots are the same as in Fig. 7. Sharpness of frequency tuning was less in these cells compared with Fig. 7. As intensity was increased, the excitatory frequency response areas expanded above and below CF. *A*: this unit had a CF of 19 kHz, a threshold of 31 dB SPL, and a Q10dB of 1.5. *B*: this unit had a CF of 15 kHz, a threshold of 24 dB SPL, and a Q10dB of 3.0.

Young and Brownell 1976). Decerebration abolishes descending inputs from auditory cortex. Because the auditory cortex sends descending inputs to the granule layer (Weedman and Ryugo 1996) that then contact cartwheel cells by the parallel fibers, eliminating this input likely has significant impact on how the cells respond to sounds. Smaller impacts may arise from anesthesia as anesthesia can reduce or eliminate complex spikes (Joris 1998; Parham et al. 2000). However, our results in awake mouse are similar to recent findings in ketamine/xylazine-anesthetized rat (Caspary et al. 2006). In our awake mouse preparation, the balance between intact auditory pathways and inhibition may have revealed the clear frequency tuning of cartwheel cells.

In addition, in this study we stressed the temporal aspects of cartwheel cell responses by plotting spectrotemporal histograms. The rationale for this type of response plot is that many cartwheel cells show complex patterns of excitation and inhibition that may mask the cell's frequency tuning when the response is measured by spike count or spike rate alone. Therefore the combination of recording responses in an awake animal and plotting response properties such that temporal and frequency information was retained in response maps, resulted in our findings of strong auditory responses in cartwheel cells. Responses of these cartwheel cells suggest that we should broaden our understanding of the DCN′s functional role in auditory processing.

The clear frequency tuning of cartwheel cells presents an interesting puzzle. Because the auditory nerve does not synapse in the molecular layer of the DCN (Merchan et al. 1985; Ryugo and May 1993), the auditory input to cartwheel cells must arrive, by auditory mossy fibers, from connections with brain stem nuclei that are not yet known or from descending projections from the auditory cortex (Weedman and Ryugo 1996) or the inferior colliculus (Caicedo and Herbert 1993; Schofield and Cant 1999). Other possibilities include input from VCN (Golding et al. 1995) or type II auditory fibers (Brown et al. 1988). The long-latency responses of cartwheel cells suggest that the auditory input is from descending projections or possibly type II auditory nerve fibers. Further study is needed to identify the dominant pathways of auditory input to cartwheel cells.

If the auditory input to cartwheel cells is from parallel fibers, then one would expect that the frequency tuning would be disperse because the parallel fibers run perpendicular to the tonotopy of the auditory nerve projections. However, in our recordings from cartwheel cells, their characteristic frequencies were near to the tonotopic tuning of the nearby cells that receive direct auditory nerve input. If the auditory input arrives by mossy fibers, then one hypothesis for the tonotopic organization is that the mossy fibers project tonotopically to the granular cell regions. This means that the cartwheel cells that are near the soma of the granule cells receive a stronger connection than the cartwheel cells that lie more distally along the parallel fibers. This would result in stronger inputs from appropriately tuned granule cells, thus explaining the tonotopy. A similar mechanism has been suggested in the cerebellum (Bower and Woolston 1983; Eccles et al. 1972), where the ascending branch of the granule cell axons may have a more effective synapse onto Purkinje cells than the synapses from parallel fibers (Cohen and Yarom 1998; Isope and Barbour

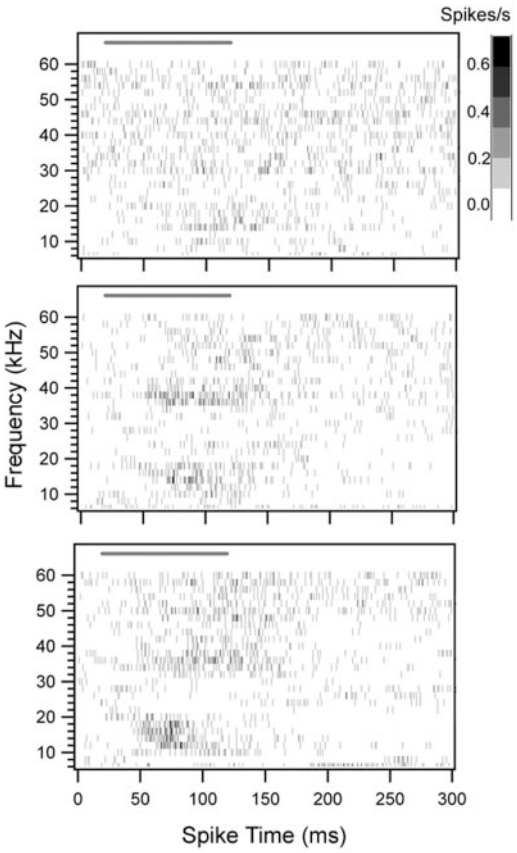

FIG. 9. Complex excitatory and inhibitory frequency response areas. Spectrotemporal histogram of a cartwheel cell with one excitatory frequency peak at 16 kHz and a second peak at 38 kHz. Details of the plots are the same as in Fig. 7. Suppression of spontaneous activity between the 2 excitatory frequency peaks suggests that inhibition separated the 2 excitatory peaks.

2002; Sims and Hartell 2006). Because cartwheel cells are the Purkinje-like cell in this cerebellum-like structure, the characteristics of the synapses may also be analogous. This similarity would help explain the tonotopic organization of cartwheel cells in the DCN.

The functional consequence of this tonotopic organization may be to emphasize the processing of auditory stimuli within isofrequency modules as cartwheel cells integrate multimodal inputs. Recurrent connections between cartwheel cells would create isofrequency modules (Golding and Oertel 1997). These modules then project along the isofrequency contours of the DCN (Berrebi and Mugnaini 1991; Manis et al. 1994) to contact fusiform cells with similar frequency tuning (Blackstad et al. 1984; Golding and Oertel 1997). Cartwheel cell inhibition of fusiform cells along isofrequency contours (Manis et al. 1994) would then integrate not only other sensory modalities, but also the delayed timings of the same frequency due to the longer latency of cartwheel cell responses. In analogy with other cerebellum-like structures, this tonotopy of cartwheel will lead to an integration of auditory stimuli in both frequency and time.

In recording responses of cartwheel cells to tones and combinations of tones, we often found complex patterns of excitation and inhibition. The functional importance of these complex patterns of excitation and inhibition in the cartwheel cells is unclear. There is compelling evidence from experiments conducted in vitro that synaptic plasticity exists at several sites within the DCN (Fujino and Oertel 2003; Tzounopoulos et al. 2004). An anti-Hebbian form of spike-timing–dependent plasticity has been observed at the synapses from parallel fibers onto cartwheel cells in the mouse DCN (Tzounopoulos et al. 2004). The synaptic plasticity at the parallel fiber synapse onto cartwheel cells could cause a cancellation of expected stimuli if the parallel fibers carried timing information about the stimuli (Roberts and Bell 2000, 2002; Roberts et al. 2006b). The complex patterns of excitation and inhibition we observed in the cartwheel cells may thus be the result of previous experience by the mouse where certain frequencies are often correlated with others. Further experiments are required to address whether adaptation of cartwheel cell responses, caused by plasticity that has been observed in vitro, actually induces the DCN to enhance important auditory patterns under natural conditions, as predicted by modeling studies (Roberts et al. 2006b). If similar plasticity of DCN responses is observed in vivo, then a compelling case could be made for the DCN playing a broad, predominant role in adaptive plasticity in the auditory system.

Our previous modeling studies (Roberts et al. 2006a) suggest that effects of spike-timing–dependent plasticity at the parallel fiber synapses onto cartwheel cells would generate a pattern of synaptic inputs that is organized in both frequency and time. To better understand how synaptic currents generate the spike patterns that we observed empirically, we constructed a numerical model of the cartwheel cell. The model demonstrated that the bimodal spike pattern does not require bimodal synaptic currents, but could be a result of the membrane currents that cause complex spikes. In addition, our numerical results suggest that the full variety of spike patterns that we observed could be parsimoniously explained by a unimodal distribution of synaptic currents. Sharply bimodal spike patterns (Fig. 3, *A* and *B*), where a narrow band of complex spikes was followed by a broad band of simple spikes, are generated by a unimodal synaptic current distribution with a sharply rising onset. Broad, unimodal spike patterns (Fig. 3, *C* and *D*) are generated by a unimodal synaptic current distribution with a slowly rising onset and a late peak. The model predicts that the duration of the synaptic current distributions greatly outlasts the stimulus duration, suggesting long delays in the parallel fiber responses to auditory stimuli.

Many cartwheel cells exhibited long-lasting inhibition, sometimes >200 ms. Inhibition of cartwheel cells could be caused by stellate cells in the molecular layer. Although cartwheel cells contact each other with glycinergic synapses, the reversal potential in cartwheel cells is such that they likely excite each other (Golding and Oertel 1996, 1997). The stellate cells are most likely excited by parallel fibers, but some of the latencies are exceedingly long to be explained by a disynaptic connection from the same parallel fibers that are exciting the cartwheel cells. One possibility for the long delay is the presence of unipolar brush cells (UBCs) in the granular cell regions of the DCN. UBCs are also present in regions of the cerebellum that receive vestibular information, and have a specialized synapse from mossy fibers that traps glutamate and leads to a prolonged postsynaptic potential in a UBC after a postsynaptic spike (Rossi et al. 1995). The axons of UBCs terminate as mossy fibers so that a prolonged activity of a UBC could drive stellate cells to inhibit cartwheel cells for the long durations observed in our recordings. The long latencies of

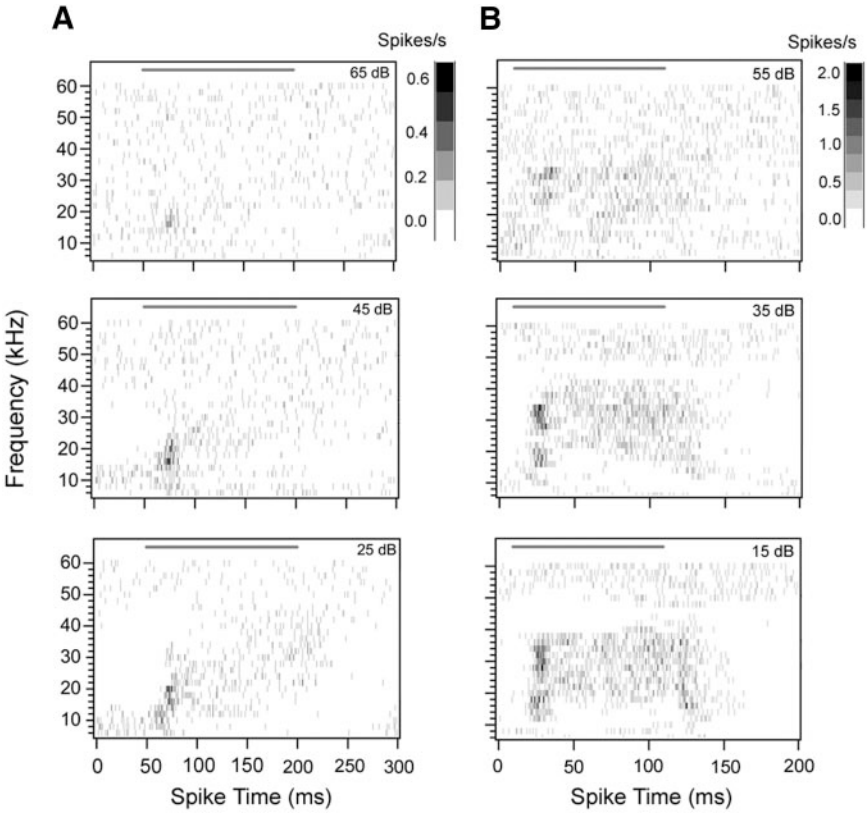

FIG. 10. Cartwheel cells have complex inhibitory frequency interactions. *A* and *B*: spectrotemporal histogram of 2 cartwheel cells that showed inhibition. Details of the plots are the same as in Fig. 7. To construct these plots, a 2-tone paradigm was used. One tone was set at the unit's CF and a second tone was presented that varied in frequency. Two tones had the same onset time and duration. Inhibition was quantified as a 20% reduction in spike rate from the rate evoked by the CF tone. Inhibition can be qualitatively observed in the spectrotemporal plots. *A*: this cell had a CF of 19 kHz and a threshold of 23 dB SPL. *B*: this cell had a CF of 32 kHz and a threshold of 25 dB SPL.

synaptic inputs to cartwheel cells, coupled with the plasticity of the DCN, could lead to learning associations between auditory stimuli and vestibular stimuli caused by slow head movements.

The function of the DCN as a filter for sound localization cues has been discussed extensively in the literature (Davis et al. 1996; Ding et al. 1999; May 2000; Oertel and Young 2004; Reiss and Young 2005; Young and Davis 2002; Young et al. 1995; Zheng and Voigt 2006). Spectral cues from the head-related transfer function are thought to be combined in the DCN with proprioceptive information to determine the location of a sound source. This filtering process is adaptive because the shape of the pinna, or the coding of proprioceptive information, could change through growth or injury. However, the DCN receives information from many parts of the brain and will therefore act as an adaptive filter to expect the auditory consequences of any sensory event (Oertel and Young 2004) and use that expectation to modify signals in the auditory pathway. Therefore any event that is consistently correlated with an

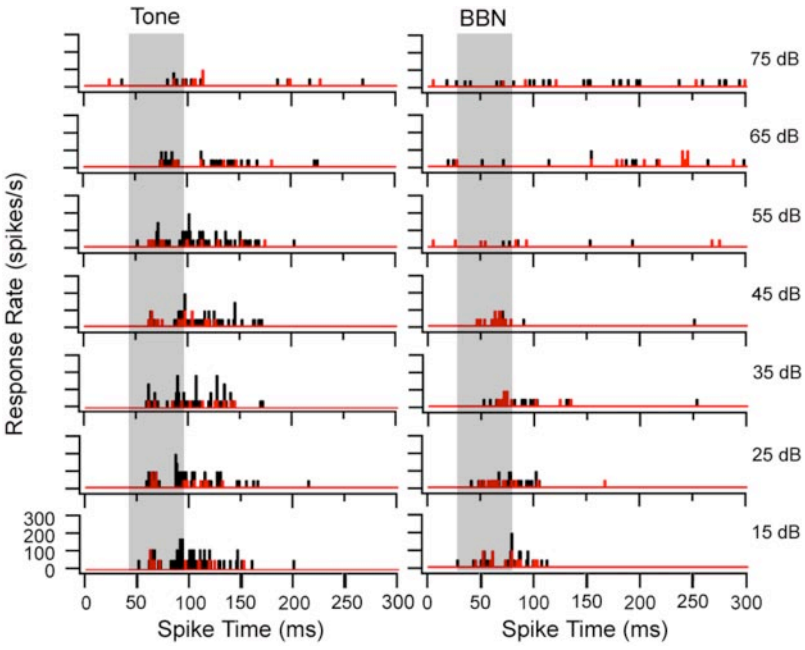

FIG. 11. Cartwheel cells responded better to pure tones than to broad band noise stimuli. Spike patterns of complex spikes (red) and simple spikes (black) evoked by CF (20 kHz) tones (*left column*) and broadband noise (*right column*) at different intensities. At 75-dB attenuation, the CF tone evoked a response from the cell but a response to broadband noise was not evoked until 45-dB attenuation. Gray vertical bar denotes the stimulus onset time and duration in all PSTHs.

auditory stimulus, whether motor or sensory (Oertel and Young 2004; Woody et al. 1992; Young and Davis 2002), could be used to filter auditory information in the DCN. The critical factor is whether information about the event is represented in parallel fibers. Our findings that cartwheel cells in the awake mouse respond well to sound and are clearly tuned in frequency suggest that auditory stimuli are strongly represented in parallel fibers of the awake mouse.

The strong representation of auditory information in the parallel fibers suggests that the cartwheel cells play a role in sound processing in addition to filtering sound localization cues. For example, the DCN may be involved in echo suppression (Kaltenbach et al. 1993; Wickesberg and Oertel 1990), vocal auditory suppression, or enhancement of auditory processing in the presence of background noise (Franosch et al. 2003; Frisina et al. 1994). An intriguing adaptive function is that responses in DCN change during classical conditioning (Beroukha et al. 1998; Woody et al. 1992); the responses of units in DCN to a conditioned stimulus (a click) are modified during an eye blink conditioning protocol. These conditioning results, coupled with the DCN′s possible involvement in filtering background noise, suggest that the DCN is involved in many other functions besides sound localization. We suggest that the general function of the DCN may be to enhance behaviorally important auditory stimuli in a changing, noisy environment.

ACKNOWLEDGMENTS

We thank R. Felix II and N. Sawtell for collecting some of the empirical data.

GRANTS

This work was supported by National Institutes of Health Grants R01-MH-60364 to P. D. Roberts and R01-DC-04733 to C. V. Portfors and National Science Foundation Grant IOB-0445648 to P. D. Roberts.

REFERENCES

Bell CC. An efference copy in electric fish. *Science* 214: 450–453, 1981.

Bell CC, Bodznick D, Montgomery J, Bastian J. The generation and subtraction of sensory expectations within cerebellum-like structures. *Brain Behav Evol* 50, *Suppl*. 1: 17–31, 1997.

Beroukha A, Gruen E, Woody CD. Facilitation of acoustic responses of cartwheel neurons of the cat dorsal cochlear nucleus. *Neuroreport* 9: 3457–3461, 1998.

Berrebi AS, Mugnaini E. Distribution and targets of the cartwheel cell axon in the dorsal cochlear nucleus of the guinea pig. *Anat Embryol* (Berl) 183: 427–454, 1991.

Blackstad TW, Osen KK, Mugnaini E. Pyramidal neurones of the dorsal cochlear nucleus: a golgi and computer reconstruction study in cat. *Neuroscience* 13: 827–854, 1984.

Bower JM, Woolston DC. Congruence of spatial organization of tactile projections to granule cell and Purkinje cell layers of cerebellar hemispheres of the albino rat: vertical organization of cerebellar cortex. *J Neurophysiol* 49: 745–766, 1983.

Brown M, Berglund A, Kiang N, Ryugo D. Central trajectories of type ii spiral ganglion neurons. *J Comp Neurol* 278: 581–590, 1988.

Caicedo A, Herbert H. Topography of descending projections from the inferior colliculus to auditory brainstem nuclei in the rat. *J Comp Neurol* 328: 377–392, 1993.

Caspary DM, Hughes LF, Schatteman TA, Turner JG. Age-related changes in the response properties of cartwheel cells in rat dorsal cochlear nucleus. *Hear Res* 216–217: 207–215, 2006.

Cohen D, Yarom Y. Patches of synchronized activity in the cerebellar cortex evoked by mossy-fiber stimulation: questioning the role of parallel fibers. *Proc Natl Acad Sci USA* 95: 15032–15036, 1998.

Davis KA, Miller RL, Young ED. Effects of somatosensory and parallel-fiber stimulation on neurons in dorsal cochlear nucleus. *J Neurophysiol* 76: 3012–3024, 1996.

Davis KA, Voigt HF. Evidence of stimulus-dependent correlated activity in the dorsal cochlear nucleus of decerebrate gerbils. *J Neurophysiol* 78: 229–247, 1997.

Davis KA, Young ED. Granule cell activation of complex-spiking neurons in dorsal cochlear nucleus. *J Neurosci* 17: 6798–6806, 1997.

Destexhe A, Mainen Z, Sejnowski TJ. An efficient method for computing synaptic conductances based on a kinetic model of receptor binding. *Neural Comput* 6: 14–18, 1994.

Ding J, Benson TE, Voigt HF. Acoustic and current-pulse responses of identified neurons in the dorsal cochlear nucleus of unanesthetized, decerebrate gerbils. *J Neurophysiol* 82: 3434–3457, 1999.

Eccles JC, Sabah NH, Schmidt RF, Taborikova H. Integration by purkyne cells of mossy and climbing fiber inputs from cutaneous mechanoreceptors. *Exp Brain Res* 15: 498–520, 1972.

Franosch JM, Kempter R, Fastl H, van Hemmen JL. Zwicker tone illusion and noise reduction in the auditory system. *Phys Rev Lett* 90: 178103, 2003.

Frisina RD, Walton JP, Karcich KJ. Dorsal cochlear nucleus single neurons can enhance temporal processing capabilities in background noise. *Exp Brain Res* 102: 160–164, 1994.

Fujino K, Oertel D. Bidirectional synaptic plasticity in the cerebellum-like mammalian dorsal cochlear nucleus. *Proc Natl Acad Sci USA* 100: 265–270, 2003.

Golding NL, Oertel D. Context-dependent synaptic action of glycinergic and gabaergic inputs in the dorsal cochlear nucleus. *J Neurosci* 16: 2208–2219, 1996.

Golding NL, Oertel D. Physiological identification of the targets of cartwheel cells of the dorsal cochlear nucleus. *J Neurophysiol* 78: 248–260, 1997.

Golding NL, Robertson D, Oertel D. Recordings from slices indicate that octopus cells of the cochlear nucleus detect coincident firing of auditory nerve fibers with temporal precision. *J Neurosci* 15: 3138–3153, 1995.

Haenggeli C-A, Pongstaporn T, Doucet J R, Ryugo DK. Projections from the spinal trigeminal nucleus to the cochlear nucleus in the rat. *J Comp Neurol* 484: 191–205, 2005.

Isope P, Barbour B. Properties of unitary granule cell→Purkinje cell synapses in adult rat cerebellar slices. *J Neurosci* 22: 9668–9678, 2002.

Izhikevich EM. Simple model of spiking neurons. *IEEE Trans Neural Netw* 14: 1569–1572, 2003.

Izhikevich EM. *Dynamical Systems in Neuroscience: The Geometry of Excitability and Bursting*. Cambridge, MA: MIT Press, 2006.

Joris PX. Response classes in the dorsal cochlear nucleus and its output tract in the chloralose-anesthetized cat. *J Neurosci* 18: 3955–3966, 1998. xy

Kaltenbach JA, Meleca RJ, Falzarano PR, Myers SF, Simpson TH. Forward masking properties of neurons in the dorsal cochlear nucleus: possible role in the process of echo suppression. *Hear Res* 67: 35–44, 1993.

Kim Y, Trussell LO. Ion channels generating complex spikes in cartwheel cells of the dorsal cochlear nucleus. *J Neurophysiol* 97: 1705–1725, 2007.

Li H, Mizuno N. Single neurons in the spinal trigeminal and dorsal column nuclei project to both the cochlear nucleus and the inferior colliculus by way of axon collaterals: a fluorescent retrograde double-labeling study in the rat. *Neurosci Res* 29: 135–142, 1997.

Manis PB, Spirou GA, Wright DD, Paydar S, Ryugo DK. Physiology and morphology of complex spiking neurons in the guinea pig dorsal cochlear nucleus. *J Comp Neurol* 348: 261–276, 1994.

May BJ. Role of the dorsal cochlear nucleus in the sound localization behavior of cats. *Hear Res* 148: 74–87, 2000.

Merchan M, Collia F, Merchan J, Saldana E. Distribution of primary afferent fibres in the cochlear nuclei. A silver and horseradish peroxidase (hrp) study. *J Anat* 141: 121–130, 1985.

Oertel D, Young ED. What's a cerebellar circuit doing in the auditory system? *Trends Neurosci* 27: 104–110, 2004.

Ohlrogge M, Doucet J, Ryugo D. Projections of the pontine nuclei to the cochlear nucleus in rats. *J Comp Neurol* 436: 290–303, 2001.

Parham K, Bonaiuto G, Carlson S, Turner JG, D'Angelo WR, Bross LS, Fox A, Willott JF, Kim DO. Purkinje cell degeneration and control mice: responses of single units in the dorsal cochlear nucleus and the acoustic startle response. *Hear Res* 148: 137–152, 2000.

Parham K, Kim DO. Spontaneous and sound-evoked discharge characteristics of complex-spiking neurons in the dorsal cochlear nucleus of the unanesthetized decerebrate cat. *J Neurophysiol* 73: 550–561, 1995.

Paxinos G, Franklin KBJ. *The Mouse Brain in Stereotaxic Coordinates* (2nd ed.). San Diego, CA: Academic Press, 2001.

Reiss LAJ, Young ED. Spectral edge sensitivity in neural circuits of the dorsal cochlear nucleus. *J Neurosci* 25: 3680–3691, 2005.

Roberts PD, Bell CC. Computational consequences of temporally asymmetric learning rules: II. Sensory image cancellation. *J Comput Neurosci* 9: 67–83, 2000.

Roberts PD, Bell CC. Spike timing dependent synaptic plasticity in biological systems. *Biol Cybern* 87: 392–403, 2002.

Roberts PD, Lafferriere G, Sawtell N, Williams A, Bell CC. Dynamic regulation of spike-timing dependent plasticity in electrosensory processing. *Neurocomputing* 69: 1195–1198, 2006a.

Roberts PD, Portfors CV, Sawtell N, Felix R. Model of auditory prediction in the dorsal cochlear nucleus via spike-timing dependent plasticity. *Neurocomputing* 69: 1191–1194, 2006b.

Rossi DJ, Alford S, Mugnaini E, Slater NT. Properties of transmission at a giant glutamatergic synapse in cerebellum: the mossy fiber-unipolar brush cell synapse. *J Neurophysiol* 74: 24–42, 1995.

Ryugo D, May S. The projections of intracellularly labeled auditory nerve fibers to the dorsal cochlear nucleus of cats. *J Comp Neurol* 329: 20–35, 1993.

Schofield B, Cant NB. Descending auditory pathways: Projections from the inferior colliculus contact superior olivary cells that project bilaterally to the cochlear nuclei. *J Comp Neurol* 409: 210–223, 1999.

Sims RE, Hartell NA. Differential susceptibility to synaptic plasticity reveals a functional specialization of ascending axon and parallel fiber synapses to cerebellar purkinje cells. *J Neurosci* 26: 5153–5159, 2006.

Tzounopoulos T, Kim Y, Oertel D, Trussell LO. Cell-specific, spike timing-dependent plasticities in the dorsal cochlear nucleus. *Nat Neurosci* 7: 719–725, 2004.

Weedman DL, Ryugo DK. Projections from auditory cortex to the cochlear nucleus in rats: synapses on granule cell dendrites. *J Comp Neurol* 371: 311–324, 1996.

Wickesberg RE, Oertel D. Delayed, frequency-specific inhibition in the cochlear nuclei of mice: a mechanism for monaural echo suppression. *J Neurosci* 10: 1762–1768, 1990.

Woody CD, Wang XF, Gruen E, Landeira-Fernandez J. Unit activity to click cs changes in dorsal cochlear nucleus after conditioning. *Neuroreport* 3: 385–388, 1992.

Young ED, Brownell WE. Responses to tones and noise of single cells in dorsal cochlear nucleus of unanesthetized cats. *J Neurophysiol* 39: 282–300, 1976.

Young ED, Davis KA. Circuitry and function of the dorsal cochlear nucleus. In: *Integrative Functions in the Mammalian Auditory Pathway*, edited by Oertel D, Fay R, Popper A. New York: Springer-Verlag, 2002, p. 160–206.

Young ED, Nelken I, Conley RA. Somatosensory effects on neurons in dorsal cochlear nucleus. *J Neurophysiol* 73: 743–765, 1995.

Zhang S, Oertel D. Cartwheel and superficial stellate cells of the dorsal cochlear nucleus of mice: intracellular recordings in slices. *J Neurophysiol* 69: 1384–1397, 1993a.

Zhang S, Oertel D. Tuberculoventral cells of the dorsal cochlear nucleus of mice: intracellular recordings in slices. *J Neurophysiol* 69: 1409–1421, 1993b.

Zheng X, Voigt HF. A modeling study of notch noise responses of type iii units in the gerbil dorsal cochlear nucleus. *Ann Biomed Eng* 34: 697–708, 2006.

Zhou J, Shore S. Projections from the trigeminal nuclear complex to the cochlear nuclei: A retrograde and anterograde tracing study in the guinea pig. *J Neuro Res* 78: 901–907, 2004.